TSCFA 台灣超臨界流體協會
Taiwan Supercritical Fluid Association

電子報第 185 期

活動訊息

◆ *論文徵稿*

即日起徵求SuperGreen2022論文，主題：

(1)**"Physicochemical properties and thermodynamics"**

(2)**"Natural products, pharmaceutical and biomedical applications"**

(3)**"Reactions, material design and nanotechnology"**

(4)**"Process intensification, CO_2 utilization and industrial applications"**

(5)**"Applications of SCF technology in Taiwan"**

等5大主題領域的研究論文，邀請各界踴躍投稿，及蒞臨與會交流。

https://supergreen2022.conf.tw/

◆ **第12屆超臨界流體國際研討會暨第21屆超臨界流體技術應用與發展研討會及會員大會**

時間：2022年**10月28~29日(星期五~六)**

地點：**集思北科大會議中心億光大樓2樓『感恩廳』**

https://supergreen2022.conf.tw/

技術專欄

◆ Supercritical Carbon Dioxide Decellularized Xenograft-3D CAD/CAM Carved Bone Matrix Personalized for Human Bone Defect Repair

團體會員介紹

◆ 綠茵生技股份有限公司

教育訓練班

◆ (日間班)高壓氣體特定設備操作人員安全衛生教育訓練班 08/15~08/19

產業新聞

◆ 亞果生醫亮眼新產品 iMist 愛眼濕 亞洲生技展搶眼亮相

資料來源：

https://money.udn.com/money/story/12331/6492742?from=edn_search_result

技術文摘

◆ A Comparative Assessment on Different Aspects of the Non-Linear Instability Dynamics of Supercritical Fluid in Parallel Channel Systems 平行通道系統中超臨界流體非線性不穩定性動力學不同方面的比較評估

◆ Discovery of Stishovite in the Prismatine-Bearing Granulite from Waldheim, Germany: A Possible Role of Supercritical Fluids of Ultrahigh-Pressure Origin 在德國瓦爾德海姆含棱晶石的花崗岩中發現 Stishovite：超高壓源超臨界流體的可能作用

◆ Experimental Investigations on Thermal-Hydraulics of Supercritical Carbon Dioxide Under Natural Circulation Vertical Flows 自然循環垂直流下超臨界二氧化碳熱流試驗研究

◆ Lipid Extracts Obtained by Supercritical Fluid Extraction and Their Application in Meat Products 超臨界流體萃取獲得的脂質提取物及其在肉製品中的應用

◆ Numerical investigation of heat transfer deterioration and the variation of Prandtl number in the main flow area under supercritical conditions 超臨界條件下主流區傳熱劣化及普朗特數變化的數值研究

◆ Production of Protein Hydrolysate from Quinoa (*Chenopodium quinoa* Willd.): Economic and Experimental Evaluation of Two Pretreatments Using Supercritical Fluids' Extraction and Conventional Solvent Extraction *從藜麥（ Chenopodium quinoa* Willd.） 中生產蛋白質水解物：使用超臨界流體萃取和常規溶劑萃取兩種預處理的經濟和實驗評估

12th International Conference on Supercritical Fluid (Supergreen 2022) Abstract Template

Author 1[a], Author 2[b,*]

[a]Author's affiliation, City, Country

[b]Author's affiliation, City, Country

*Corresponding author: E-mail address

This is the abstract template for the 12th International Conference on Supercritical Fluid (Supergreen 2022). Please follow these instructions to prepare your abstract.

1) Page format

Prepare **one page** abstract in **A4-size**. Top, bottom, right and left margins are set to **25.4 mm**. 'Times New Roman' or similar fonts are used throughout the abstract.

2) Title

Title should be **centered** and presented in **14 pt, bold** with a fixed line spacing of **20 pt**. Leave one-line space after the title. The first letter of words in title should be capitalized except for articles, short prepositions, and conjunctions.

3) Author name(s)

Author name(s) are centered and presented in **12 pt** with a fixed line spacing of **20 pt**. The corresponding author should be labelled with '*' and the presenting author should be underlined.

4) Affiliation(s)

Affiliations are centered and presented in **10 pt** with a fixed line spacing of **20 pt**. Leave one-line space after the affiliation.

5) Abstract

Abstract is presented in **12 pt** with a fixed line spacing of **20 pt**. The text should be **justified left and right**. Figures and tables could be included in the abstract with the sequential numbering. All figures and tables are accompanied with a caption.

TSCFA

第12屆超臨界流體國際研討會
暨 第21屆超臨界流體技術應用與發展研討會
111年度會員大會

2022-10-28～29

SuperGreen 2022

指導單位 |
MOST 科技部

主辦單位 |
TSCFA 台灣超臨界流體協會
TAIPEI TECH 國立臺北科技大學

親愛的貴賓 您好：

　　台灣超臨界流體協會謹訂於民國111年10月28日(星期五)至10月29日(星期六)，
假　集思北科大會議中心億光大樓 2 樓 『 感恩廳 』，舉辦「 SuperGreen 2022
第12屆超臨界流體國際研討會暨第21屆超臨界流體技術應用與發展研討會」，
並於10月29日下午14時舉行111年度會員大會。 恭請

蒞臨指導

SuperGreen 2022國際研討會暨第21屆技術研討會
及年會籌備會主任委員　謝達仁　王錫福
副主任委員　廖盛焜　蘇至善
台灣超臨界流體協會 全體理監事暨籌備會委員

敬邀

111年度活動議程

時　　間		議　程　內　容
10月28日（星期五）	8:30 - 17:30	報到
	09:20 - 9:30	開幕式
	09:30 - 12:10	大會 & 專題演講
	12:10 - 13:00	午餐 / 聯誼時間
	14:00 - 17:30	大會 & 專題演講
	18:30 - 21:00	聯誼晚宴
10月29日（星期六）	09:00 - 11:55	大會 & 專題演講
	12:00 - 12:10	閉幕式 & 頒獎
	12:30-14:30	111年度會員大會

第 １ ２ 屆 超 臨 界 流 體 國 際 研 討 會
暨第 21 屆超臨界流體技術應用與發展研討會及會員大會

□ 參加研討會 □參加會員大會 (可重複勾選)

公 司/學校名稱			報名日期	年　月　日
會 員 別	□團體會員 □個人會員 □學生會員 □非會員		聯 絡 人	
地　　址	□□□		電　　話	（ ） 分機

姓　　名	職　　稱	E-mail	活動項目及午餐	
(中)			10/28 □午餐 □晚宴　□不用餐	
(英)			10/29 □午餐 □不用餐 □素食者	
(中)			10/28 □午餐 □晚宴　□不用餐	
(英)			10/29 □午餐 □不用餐 □素食者	

活動費用		
	Early Before September 30 2022	Late and On-site After September 30 2022
Online participant	NTD $3,000 (外籍 USD $100)	NTD $4,500 (外籍 USD $150)
Regular participant	NTD $7,500 (外籍 USD $250)	NTD $9,000 (外籍 USD $300)
TSCFA member	NTD $3,000	NTD $4,500
Student	NTD $2,000	NTD $3,000

費用包含：2 天茶點、午餐、晚宴、研討會論文摘要集等，**只參加一天恕不退費**。

※本表如不敷使用，請自行新增，亦可透過會議網站報名，網址：**https://supergreen2022.conf.tw/**

★上述個人資料本會僅作為此次活動相關服務使用，絕不另作其他用途。特此聲明！

備註：

➢ 為統計參加人數及確定餐點數量，務必請於**研討會(10/15)**前完成報名手續。

➢ 報名表請 **e-mail** 至協會，完成報名手續後，本會將製作出席證，出席證於當日報到時領取。

➢ **活動地點**：**集思北科大會議中心億光大樓 2 樓『感恩廳』**。(台北市大安區忠孝東路三段 1 號)

➢ **晚宴地點**：暫定「美麗信花園酒店」(台北市中山區市民大道三段 83 號)。

➢ **住宿**：如需住宿者，可參考此次研討會配合飯店，可享有專案費用，請填寫訂房單，由秘書處統計，並代為訂房，亦或直接填寫 google 表單 https://forms.gle/dFKXaSsDMkmUBTZW7。

➢ 協會聯絡人：吳家瑩小姐，電話：(07)355-5706，E-Mail：tscfa@mail.mirdc.org.tw

➢ **付款方式**：
1. 郵局劃撥帳戶：台灣超臨界流體協會；帳號：42221636
2. 銀行匯款戶名：社團法人台灣超臨界流體協會，兆豐國際商銀-港都分行(代碼：017)；
帳號：002-09-01847-9 (若以 ATM 轉帳請告知您的姓名及轉帳帳號末五碼以便查對)
3. 線上付款：可由會議網址報名及繳費 **https://supergreen2022.conf.tw/**

集思北科大會議中心
gis TAIPEI TECH convention center

地址：台北市忠孝東路3段1號 億光大樓2-3樓 (197號旁邊)

電話：02-2741-7655#201~202

傳真：02-2741-8699

捷運

1. From airport to Zhongxiao Xinsheng Station (BL14)

Taipei Songshan Airport	MRT BR approx. 8 min.	Zhongxiao Fuxing Station	MRT BL approx. 2 min.	Zhongxiao Xinsheng Station
Taoyuan International Airport	Taoyuan Airport MRT approx. 40-55 min.	Taipei Main Station	MRT BL approx. 4 min.	

2. From Zhongxiao Xinsheng Station (BL14) Exit 4 to Gis Taipei Tech by walk

Sec. 1, Xinsheng S. Rd

Sec. 1, Jianguo S. Rd.

Zhongxiao Xinsheng Station (BL14)

Exit 4

TAIPEI TECH

P Underground Parking

Everlight Building

Gis Taipei Tech

Sec. 3 , Zhongxiao E. Rd.

Go straight by walk (about 8 minutes)

1.億光地下停車場：

建國南路一段(往建國北方向)，過忠孝東路三段即可於右手側看見停車場入口

平日: 40元/每小時

假日: 50元/每小時

*收費如有不同，依停車場現場公告為主

停車資訊

第12屆超臨界流體國際研討會暨第21屆超臨界流體技術應用與發展研討會及會員大會

訂房單

優惠日期：2022年10月27日(四)至2022年10月28日(五)，共2天

□新增	□修改	□取消

姓名：	性別：□男　□女

入住日期：2022/10/	退房日期：2022/10	天數：　　晚

電話/手機：	E-mail/傳真：

發票抬頭：	發票統編：

是否開車：	備註：

優惠房價表

房型	床型尺寸	間數	房價	小計	坪數及特色
標準大床房	1,630 x 1,970mm		NT$2,600		6.9坪，無浴缸，每層1間
好萊塢雙床房	2小床合併 (2,460 x 2,000mm)		NT$2,700		7.8坪，標準雙床的合併版本，無浴缸
標準雙床房	1,230 x 1,970mm		NT$2,700		7.8坪，無浴缸

總計：NT$_____元(費用內含稅及服務費)

■ 因標準大床房、好萊塢雙床房數量較少，將依回單順序提供，滿房將安排標準雙床房。

■ 入住時間：下午3:00，退房時間：中午12:00。

■ 請於退房當日將全額款項結清。

客房專屬優惠如下：

● 免費使用 2F Lounge和17F大浴場。

● 全館免費無線上網服務。

● 房內每日4瓶礦泉水。

● 美國市佔率第一Serta® 舒達飯店專用床墊。

● 免費停車：入住當日下午14:30-退房當日12:30，超過費用為：半小時$30元，當日最高$250元。

➤ 早餐為中西日式自助餐，**需另外支付**，金額原價每位$660，本次可提供**優惠價 $500**。(至多2位)

➤ 當天臨時變更、取消房間費用不予退還，以入住第一晚房費計算。

MGH Mitsui Garden Hotel 台北忠孝

MGH 和苑三井花園飯店 台北忠孝 特約停車場介紹

台北科技大學
National Taipei University of Technology

LEXUS

日月光
億光大樓

忠孝東路三段 Zhongxiao E. Rd.

MRT 忠孝新生
3號出口

和苑三井花園飯店 台北忠孝
MGH Mitsui Garden Hotel Taipei Zhongxiao

※房客於住宿期間免費停車 入住當天 15:00～退房日 12:00 止

機械式停車場　飯店 B1

平面停車場　步行 6 分

永吉豐停車場（66 台）

營業時間：24 小時　車高限制：1.9m

平日: $60 /時　當日最高收費：$250

假日: $80 /時　當日最高收費：$350

日月亭億光大樓停車場（125 台）

營業時間：24 小時　車高限制：2.1m

平日: $40 /時　當日最高收費：$200

假日: $50 /時　當日最高收費：$250

※如超出折抵時間，需自行付費。

Article

Supercritical Carbon Dioxide Decellularized Xenograft-3D CAD/CAM Carved Bone Matrix Personalized for Human Bone Defect Repair

Meng-Yen Chen [1], Jing-Jing Fang [2], Jeng-Nan Lee [3], Srinivasan Periasamy [4], Ko-Chung Yen [4], Hung-Chou Wang [4] and Dar-Jen Hsieh [4,*]

[1] Division of Oral and Maxillofacial Surgery, Department of Stomatology, College of Medicine, National Cheng Kung University, Tainan 704302, Taiwan; ccdc0002.tw@gmail.com

[2] Department of Mechanical Engineering, College of Engineering, National Cheng Kung University, Tainan 701401, Taiwan; fangjj@mail.ncku.edu.tw

[3] Department of Mechanical Engineering, Cheng Shiu University, Kaohsiung 833301, Taiwan; jengnan@gcloud.csu.edu.tw

[4] R & D Center, ACRO Biomedical Co., Ltd. 2nd. Floor, No.57, Luke 2nd. Rd., Luzhu District, Kaohsiung City 821011, Taiwan; srini@acrobiomedical.com (P.S.); hearty_max@acrobiomedical.com (K.-C.Y.); oscar@acrobiomedical.com (H.-C.W.)

* Correspondence: dj@acrobiomedical.com

Abstract: About 30–50% of oral cancer patients require mandibulectomy and autologous fibula reconstruction. Autograft is the gold standard choice because of its histocompatibility; however, it requires additional surgery from the patient and with possible complications such as loss of fibula leading to calf weakening in the future. Allograft and xenograft are alternatives but are susceptible to immune response. Currently, no personalized bone xenografts are available in the market for large fascial bone defects. In addition, a large-sized complex shape bone graft cannot be produced directly from the raw material. We propose the use of porcine bones with 3D CAD/CAM carving to reconstruct a personalized, wide range and complex-shaped bone. We anticipate that patients can restore their native facial appearance after reconstruction surgery. Supercritical CO_2 ($SCCO_2$) technology was employed to remove the cells, fat and non-collagenous materials while maintaining a native collagen scaffold as a biomedical device for bone defects. We successfully developed 3D CAD/CAM carved bone matrices, followed by $SCCO_2$ decellularization of those large-sized bones. A lock-and-key puzzle design was employed to fulfil a wide range of large and complex-shaped maxillofacial defects. To conclude, the 3D CAD/CAM carved bone matrices with lock and key puzzle Lego design were completely decellularized by $SCCO_2$ extraction technology with intact natural collagen scaffold. In addition, the processed bone matrices were tested to show excellent cytocompatibility and mechanical stiffness. Thus, we can overcome the limitation of large size and complex shapes of xenograft availability. In addition, the 3D CAD/CAM carving process can provide personalized tailor-designed decellularized bone grafts for the native appearance for maxillofacial reconstruction surgery for oral cancer patients and trauma patients.

Keywords: maxillofacial reconstruction; supercritical CO_2; collagen bone matrix; 3D carved bone; cytocompatibility

1. Introduction

Bone grafting is an operating technique that has been employed to enhance the healing process by replacing the lost bone with material from the patient's own body, an artificial, synthetic, or natural substitute, mainly in the fields of orthopaedics, neurosurgery and plastic surgery. Bone grafts are the materials employed for filling cystic defects, for bone fractures and arthrodesis treatment, for traumatic bone defects and for the loss of bone lesions that happens after surgical removal of cancer [1]. Different types of bone grafting materials are currently used, such as autografts, allografts, synthetic variants, xenografts, alloplastic grafts, ceramic-based bone graft substitutes and polymer-based bone graft substitutes [2].

Autologous bone grafting comprises using bone obtained from the same individual recieving the graft. It is considered the "gold standard" for bone grafting because there is less risk of graft rejection, and good osteoinductivity and osteogenicity, as well as osteoconductivity. The drawback of autologous grafts is that they require additional surgery [2,3]. Allografts are obtained from humans and harvested from patients other than the one receiving the bone graft. They need sterilization and deactivation of proteins found in bone, performed using a demineralizing agent such as hydrochloric acid which degrades mineral contents. Xenografts are bone grafts derived from a non-human species, such as porcine and bovine [2]. However, xenografts are neglected because of their highly immunogenic, inadequate biomechanical qualities and foreign body adverse reaction [4]. These drawbacks of the xenografts can be overcome using decellularization techniques, mainly supercritical carbon dioxide ($SCCO_2$) which can completely nullify the cons of the xenografts [5].

The $SCCO_2$ technology can resolve the drawbacks of the decellularization of bone. Meanwhile, the $SCCO_2$ extraction technology works based on using supercritical fluid CO_2 as the extracting fluid to eliminate the fats, cells and non-collagenous proteins from the bone. The pros of $SCCO_2$ extraction technology are that it is natural, safe, non-toxic, non-corrosive, non-flammable, easily accessible and cost-effective. The vital parameters of $SCCO_2$ extraction technology are its mild critical coordinates, including pressure at 7.38 MPa and temperature at 31 °C, which can be attained effortlessly and are appropriate for bone materials. The $SCCO_2$ technology has been employed for removing lipids from bone, due to its outstanding solvent capacity for lipids; in addition, this technique significantly decreases the antigenicity during bone decellularization while preserving the strength of the bone, similar to that of the original native bone [5]. We have successfully decellularized bone, skin, cartilage and cornea using this $SCCO_2$ extraction technology [6]. The biomaterials decellularized using $SCCO_2$ extraction technology are highly biocompatible and non-toxic, with enhanced regenerative capability; most importantly without antigenicity and immunogenicity [6,7].

The bone grafts currently available in the market are produced by a technique called high-temperature sintering (300–1300 °C), to completely remove zoonotic infectious and immunogenic agents present in the bone. The high-temperature sintering destructs the intrinsic collagen components in the bone and alters the native porous structures of the bone. In addition, this technique converts the native bone materials into inorganic hydroxyapatite and tri-calcium phosphate, which is much less bioabsorbable relative to native bone [8–10].

Oral carcinoma was reported with an incidence rate of 4% of all cancers in the western world [11]. Among the oral cancers, squamous cell carcinoma is the most dominant type of cancer that affects the buccal cavity, and 49% mandibular involvement in cancer patients [12,13]. Oral cancer alters the face by frequently mutilating, and simultaneous cancer resection can lead to overwhelming cosmetic and functional loss leading to psychological, physical, functional and nutritional effects. To overcome this, craniofacial reconstruction is performed, which creates exceptional challenges because of the three-dimensional (3D) shape of the planned construction of the bone for the pivotal significance of re-establishing speech, swallowing, mastication and symmetrical facial contour. Moreover, the results of the reconstruction are frequently unpredictable

and learning-curve dependent, making pre-operative scheduling tough for reconstructive surgeons [13,14].

The conventional protocol for maxillofacial bone grafting includes multifaceted stages which are expensive, time-consuming, extremely traumatic for the patient and depend on the skills of the maxillofacial surgical team [15]. The intricacy of conservative maxillofacial prosthodontics manufacture needs many weeks and many clinic visits by the patient to try the grafts, and functional and aesthetic adjustments [16]. Most patients do not opt for subsequent surgical correction, and the degree of their defects induces a lack of self-confidence, impairing their daily activities and social lives [17]. Computer-aided design (CAD) is an innovative technology that offers advantages in the development and execution of inspiring bone graft production for traumatic and oncological craniofacial reconstructions [18]. CAD is a multifaceted and sophisticated pre-operative course. CAD starts with the acquisition of a patient's craniofacial skeleton with a 3D rendered, 64-slice high-resolution CT scan [17,19–21]. In the production of 3D customized scaffolds using numerous materials and techniques, with precise imaging methods, the design and construction of CAD-CAM scaffolds has become a straightforward method [19]. Investigations involving the customised scaffolds for alveolar ridge augmentation revealed well established positive outcomes [20,22,23].

The purpose of the current study was to evaluate the $SCCO_2$ decellularized -CAD-CAM facilitated 3D Lego jaw bone production and to assess its in vitro biocompatibility. Most of the previous studies focus on the production of a certain part of the jaw. However, in the present study, we hypothesise producing the whole jaw using $SCCO_2$ decellularized porcine bone matrices to construct a Lego form of the complete jaw.

2. Materials and Methods

2.1. 3D Mandibular Model Construction

The patient was diagnosed with a tumour located in the oral cavity. Computerized tomography (CT) from GE MEDICAL SYSTEMS with 1 mm slice thickness was used. As shown in Figure 1A,B, the DICOM imaging was decoded first and then reconstruct to a three-dimensional mandibular model by our-developed software. The OSP (Optimal Symmetry Plane) was automatically generated by locating the one and only symmetry plane which contains the maximal voxel pairs of the collateral parts [24]. The OSP was used for mirroring the right and left sides of the mandible to the other side (Figure 1C). Surgeons determined the region of the tumour located on the mandible (Figure 1D), and the mirror mandible was used to replace the tumour region (Figure 1E). Since mild facial asymmetry is common in adults, a gap usually exists between the condyle processes from the original left and the mirrored right. To adjust the positions of the mirrored half-right mandible model on-screen to overlap the original condyle processes on the left side, a complete symmetry mandible template was created (Figure 1F). If the tumour was located across the centre part of the mandible, a database of the mandibular model from patients who took orthognathic surgery was involved. The smoothing technique was then applied to generate C^2 continuity between the donor and the replacement parts.
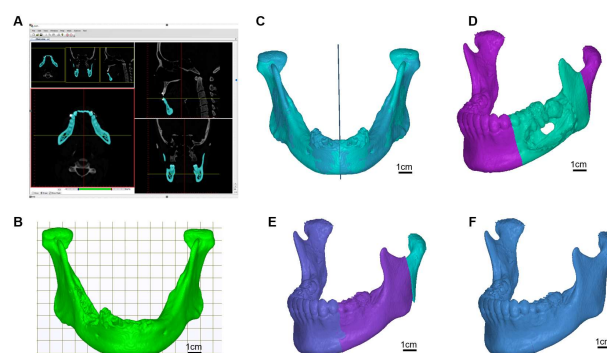
Figure 1. Scan image deciphering and 3D image generation. (**A**) Imaging decoding and model reconstruction software, (**B**) mandible model, (**C**) find the optimal symmetry plane and mirrored model, (**D**) locate the cancer region, (**E**) replace the cancer region with region mirrored part, (**F**) target template.

The resection guide and puzzle container: The osteotomy guide is mainly used to assist the tumour resection. The original mandible model was invoked for further resection guide, puzzle parts, and its container design. A guide plate with a selective thickness was generated on the surface of region indication by our-developed software, to cover the region of resection on the mandible decided by the surgeon (Figure 2). Two ends of grooves for bone sawing were made on the container to indicate the edges of resection. It was provided for the surgeon to be used during operation in assisting precise tumour resection. Functions of the resection guide were not only used for precise resection but also to ensure the implanted bone grafts puzzles were securely placed and reform the curved shape of the mandible in origin.
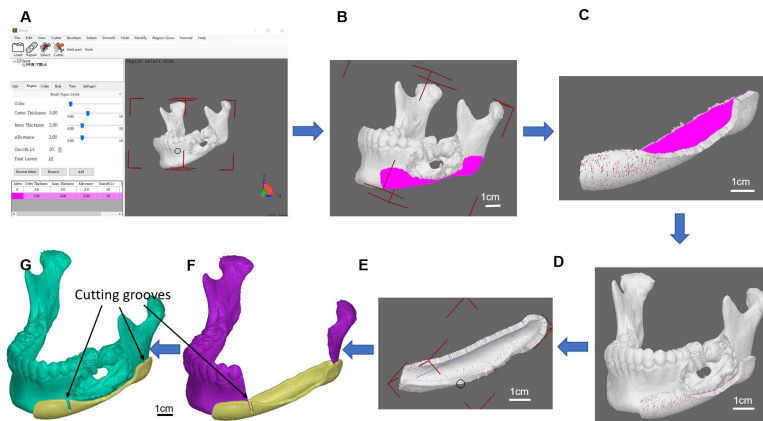

Figure 2. Osteotomy guide model. (**A**) Our developed osteotomy guide software, (**B**) container region, (**C**) generates a container with a selective thickness, (**D**) defect mandible with the container, (**E**) container refinement, (**F**) grooves of the resection guide, (**G**) cutting guide with the defect mandible model.

2.2. Osteotomy Guide Fabrication and Multi-Piece Puzzle Setup

To provide precise tumour resection and bone grafts placement, the developed software was able to construct connection latches to fasten bone graft puzzles together. The target template for the defect replacement region was segmented into many pieces of lengths of less than 2 cm which allow bone fusion between the cutting face of the mandible and the porcine bone grafts (Figure 3). Many pieces of bone grafts work like a curved combination of many pieces of puzzles to form a template mandible, latching in between connect one groove and one hole at the two-end faces attached to each piece (Figure 4). The prerequisite is that such customized materials and fabricated bone pieces must meet the requirements of the quality measurement system of classes II and III. The tumour resection guide was categorized as class II, which was fabricated by the 3D printer and bio-compatible resin.
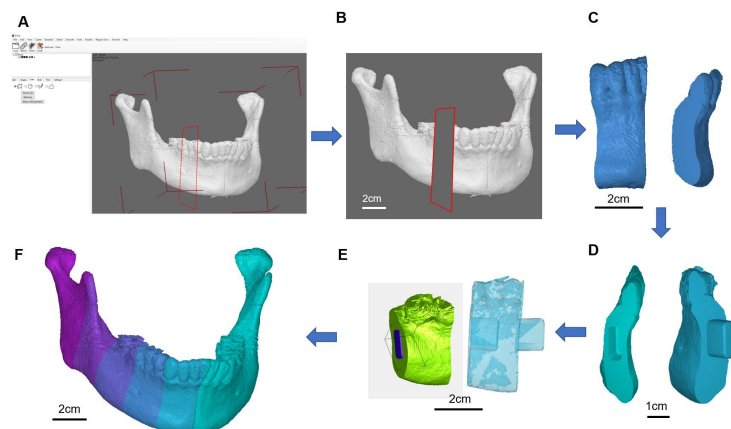
Figure 3. Multipiece Lego design. (**A**) Multi-piece design software, (**B**) selective length of one of the puzzle pieces, (**C**) puzzle piece, (**D**) latched puzzle pieces, (**E**) model views with and without transparency, (**F**) full mandible with 6 puzzle pieces on the right side of the mandible model.
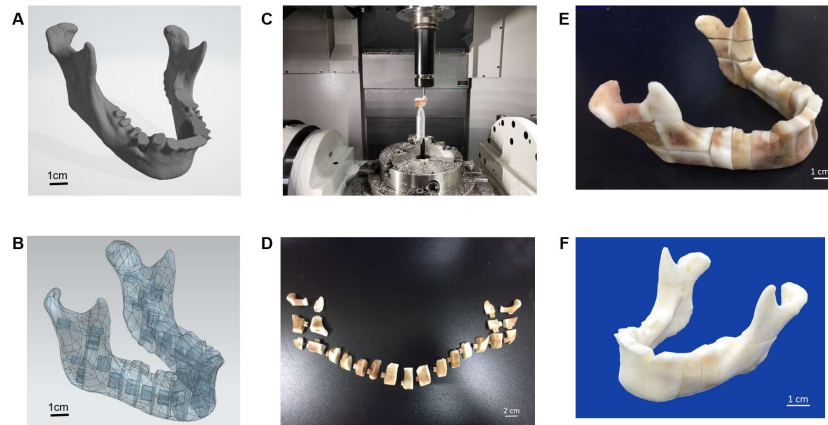
Figure 4. Five-axis CNC machining for the 3D bone for the defect repair, (**A**) STL file of the jaw bone, (**B**) geometric model of jaw bone Lego design by multiple splicing, (**C**) Five-axis CNC machining of the bone, (**D**) Lego jaw bone before arranging, (**E**) Lego jaw bone after arranging, (**F**) Lego jaw bone after cleansing with hydrogen peroxide.

2.3. Cutting and Milling a Set of Multi-Piece Lego Assembly for Defect Replacement

The porcine bone block was the basic material of the carved bone matrices. A5-axis Computer Numerical Control (CNC) CT-350 machine integrated with the controller, SIEMENS 840Dsl, was used to manufacture the carved bone puzzles. The Productivity + ™ Active Editor Pro tool probe software was employed for measurement path planning in pre-processing. The process was to check both the remaining quantity after machining and machining accuracy and efficiency. At first, a special design of bone matrices metal jig was fabricated by the CNC machine. Since the porcine material is porous and brittle, the complex geometric shape increases the complicatedness of machining. Therefore, a series of associated numerical control parameters to be used in the CNC milling should be carefully examined. We developed an associated five-axis post-processing programming control to handle such complicate applications. A template mandible with 23 connective pieces was selected to fulfil the prototype. To evaluate the accuracy of the design, we used the Renishaw OMP400 line measurement system for accuracy before assembling it into a complete mandible.

2.4. Porcine Bone Preparation

Porcine bone was purchased from Tissue Source LLC. The bones were subjected to preliminary processing such as the removal of peripheral muscle tissue and fat. The porcine bone was washed with phosphate-buffered saline (PBS). The bone was 3D CAD/CAM cut to an appropriate size according to the process design, and the skull bone block was subjected to the $SCCO_2$ process and further testing.

2.5. The $SCCO_2$ Decellularization of Bone Blocks

The bone blocks were placed on a tissue holder and placed inside a $SCCO_2$ vessel system (Helix SFE Version R3U, Applied Separations Inc., Allentown, PA, USA) with a co-solvent of 60–95% ethanol. The $SCCO_2$ process was operated at 350 bar and 35–40 °C for 80 min to decellularize the bone blocks.

2.6. Fat Analysis of $SCCO_2$ Decellularized Porcine Bone Blocks

Bone sample 100 mg powder was added to 500 μL filtered Oil red O (2.1 mg/mL) solution and incubated at room temperature for 15 min. The Oil red O solution was washed off by vortexing with distilled water twice. An amount of 250 μL of isopropanol (100%) was added to the washed sample, vortexed and incubated at room temperature for 5 min. The Blank was performed without a bone sample. The supernatant, 100 μL was taken to measure the fat in a microplate reader at 490 nm.

2.7. Hematoxylin and Eosin Staining of SCCO2 Decellularized Porcine Bone Blocks

Haematoxylin stains the nucleus of the cell displays a deep blue-purple colour, and eosin stains the protein of cytoplasm and extracellular matrix a pink colour. The native bone and decellularized bone blocks were fixed in 4% buffered formaldehyde at room temperature overnight, dehydrated stepwise and embedded in paraffin. The paraffin-embedded bone sections were cut to a thickness of 5 μm, mounted on the glass slides, fixed and stained with haematoxylin and eosin (H&E) to assess the completion of decellularization. Photographs were recorded under a microscope (Olympus bx53) for further evaluation.

2.8. Collagen Staining by Masson's Trichrome Stain of SCCO2 Decellularized Porcine Bone Blocks

After fixing and dehydrating the decellularized bone blocks with 4% formaldehyde, the paraffin-embedded bone sections were cut to a thickness of 5 μm, mounted on the glass slides, fixed and stained with Masson's trichrome stain to observe the collagen distribution in the bone.

2.9. Collagen Quantification by Estimating Hydroxyproline of SCCO2 Decellularized Porcine Bone Blocks

The concentration of collagen in the bones was analysed by estimating the hydroxyproline content using (the BIO VISION) reagent to quantify the collagen content of the bone sample. The bone samples were homogenized by adding 100 μL of ddH$_2$O and then 100 μL of HCl (~12N) for hydrolysis, incubated at 120 °C for 3 h and centrifuged at 1000× g for 3 min. Chloramine T was allowed to stand at room temperature for 5 min and 100 μL of DMAB was added for 90 min at 60 °C. The hydroxyproline standard was diluted to 0.1 mg/mL, and 0, 2, 4, 6, 8 and 10 μL were taken out and the standard curves of hydroxyproline concentration of 0, 0.2, 0.4, 0.6, 0.8 and 1 mg/mL were drawn; then the samples measured by 560 nm in a microplate reader.

2.10. DNA Quantification and Agarose Gel Electrophoresis of SCCO2 Decellularized Porcine Bone Blocks

The bone blocks (n = 3 each) were processed and extracted for genomic DNA employing a commercially available kit (NautiaZ Tissue DNA Mini Kit, Nautiagene). The DNA extracted was measured employing a microplate reader at 260 nm. The amount of residual DNA and fragment size in the bone blocks were determined by agarose gel electrophoresis.

2.11. Electron Microscopy of SCCO2 Decellularized Porcine Bone Blocks

The fixed and dehydrated bone block samples were air-dried in a clean chemical hood. The dried bone samples were glued to the aluminium table using a carbon double tape, and then the gold particles were sprayed using Hitachi E1010 Ion Sputter for scanning electron microscopy using Hitachi S-3400N scanning electron microscope for observation. Photomicrographs were recorded for analysis.

2.12. Stress Analysis of the Decellularized Bone Blocks

The biomechanical testing was performed using an MTS testing machine (MTS 858 Mini Bionix® II Biomaterials Testing System, Eden Prairie, MN, USA). The decellularized bone block samples were placed on a specially designed platform with a self-aligning function to ensure vertical compression. The sampling frequency was set at 500 Hz with a probe diameter of 2.0 mm. A pre-load of 2 Mpa with 30 s of accommodation time followed by a continuous and progressive load at a rate of 2 mm/min was applied. The first peak force detected during the test was recorded as the ultimate strength. The displacement versus force was recorded to calculate the maximal load. Maximal load in Newtons, stiffness in Newtons/mm and energy to the maximal load in millijoules were measured and recorded.

2.13. Cell Adhesion and Growth Analysis on the Decellularized Bone Blocks by SEM

Decellularized bone blocks were placed in 24 well-plates. The cell density of MG63 cells was 1 × 10^6 cells/mL was added 1ml of cell solution per well directly onto the bone blocks. After overnight (16h) incubation, the samples were washed with PBS several times, then transferred to a new 24 well-plate, 2ml DMEM-10% FBS medium was added for culturing. After Day 4, the samples were

washed with dPBS several times, then transferred to a new 24 well-plate and 2 mL of DMEM-10% FBS medium was added to continue the culture. On Day 7, the samples were washed with PBS several times, then transferred to a new 24 well-plate, 2.5% glutaraldehyde was added and fixed overnight (16 h) at 4 °C. Samples were then dehydrated in 50%, 60%, 70%, 80%, 90% and 95% ethanol for 15 min each, followed by 99.5% ethanol for 15 min twice and freeze-dried. Bone blocks were fixed on carbon tape and sprayed with platinum for SEM scanning.

3. Results

3.1. 3D Tissue Model Reconstruction and Lego Jaw Bone Carving Using 5 Axis CNC Machine

The CT scan image was decoded, and the mandibular jaw was reconstructed using model reconstruction software. The mandible was modelled to find the optimal symmetry of the plane and a mirror model was generated. The tumour area in the jaw was located and the cancer region was replaced with the mirrored area. Finally, the template of the mandible was created (Figure 1).

Using our in-house osteotomy guide software, the container region was designed and the container region modelled. In addition, the thickness of the container was selected as the option in the software. The defect mandible with the container was aligned and modelled, and the refinement was carried out. The cutting grooves were generated using the software. Finally, the cutting guide with the defect mandible was modelled (Figure 2).

The multi-piece design software was employed to select the length of individual pieces along with puzzle pieces including latched puzzle pieces. To finish, we can visualize the model views with and without transparency. All the designed individual pieces of a puzzle piece and latched puzzle pieces were designed to form a full mandible with six puzzle pieces on the right side of the mandible model (Figure 3).

We used the Geomagic Studio software to delete and remove the abnormal grid and reconstruct it into an IGES file. After the STL file was transferred to the IGES, it was integrated using the NX software, and the geometry of the defect was divided into multiple heterogeneous bones in a Puzzle-to-Latch design/lock and key design. Finally, the pieces were carved using a five-axis CNC machine into 23 pieces and cleansed using hydrogen peroxide to form a complete jaw (Figure 4).
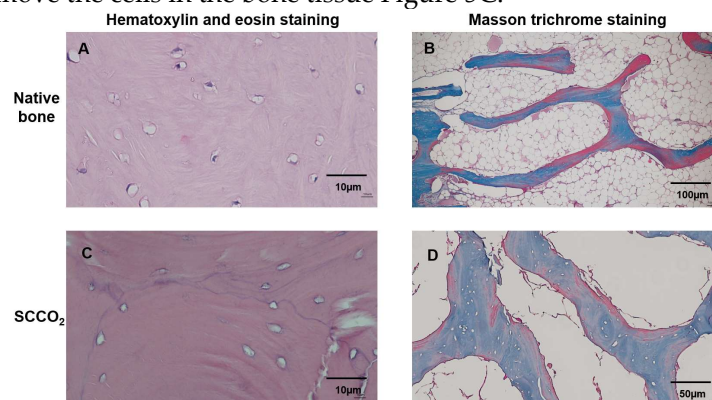
3.2. Characterization of SCCO$_2$ Derived Bone Blocks

3.2.1. Fat Content

The results of the fat content of the SCCO$_2$-processed bone blocks showed an optical density of 0.357 ± 0.024 (n = 3) at 490 nm, which is well below the acceptable range of <0.6, therefore the SCCO$_2$-processed bone blocks were qualified to be a medical device according to ISO standards.

3.2.2. H&E Staining

The H&E staining of the SCCO$_2$-processed bone blocks showed no nucleus or cell debris indicating complete decellularization, whereas nucleus and cell staining was visible in the native porcine bone Figure 5A. The results show that the decellularization process can effectively remove the cells in the bone tissue Figure 5C.

Figure 5. Characterization of SCCO$_2$-processed bone blocks by haematoxylin and eosin staining and Masson trichrome staining of the native bone block (**A,B**) and SCCO$_2$-processed bone blocks (**C,D**).

3.2.3. Masson Trichrome Staining

The decellularization of the bone blocks and retaining ECM of the bone tissue were evaluated by Masson trichrome staining. The native porcine bone contained cells and collagen were stained (Figure 5B), whereas the SCCO$_2$-processed bone blocks showed no cells; however, all the collagen was well preserved (Figure 5D), indicating the SCCO$_2$ process did not alter the ECM and collagen of the bone tissue. The collagen content was quantified in the SCCO$_2$-processed bone blocks showed 293.37 ± 22.49–335.07 ± 82.11 µg/mg of bone decellularized bone tissue with a percentage of 29–34%.

3.2.4. Residual DNA Content

The content of DNA was analysed by quantification and agarose gel electrophoresis to confirm the decellularization of the bone blocks by SCCO$_2$ technology. Three minimum criteria for optimal and successful decellularization are: (1) tissue samples should contain < 50 ng of dsDNA per mg of dry ECM, (2) any remaining DNA fragments should be smaller than 200 base pairs, and (3) the tissue should not have visible nuclear material when stained with DAPI or haematoxylin and eosin. DNA quantification of SCCO$_2$-processed bone blocks showed an average of 4.17 ng/mg of DNA (Figure 6A) which is well below the permissible level of 50 ng/mg residual DNA content for medical implant devices according to the Biological Evaluation of Medical Devices—Part 1 (ISO 2018). In addition, agarose gel electrophoresis revealed no DNA band in the SCCO$_2$-processed bone blocks, whereas DNA bands with fragment length were detected in the native porcine bone Figure 6B.
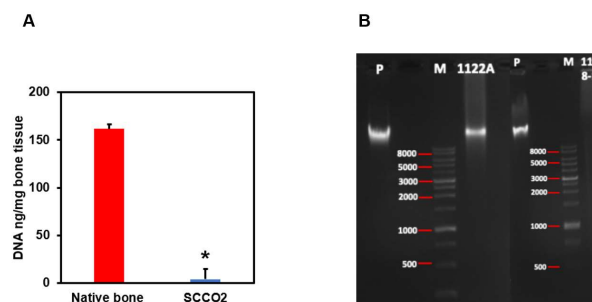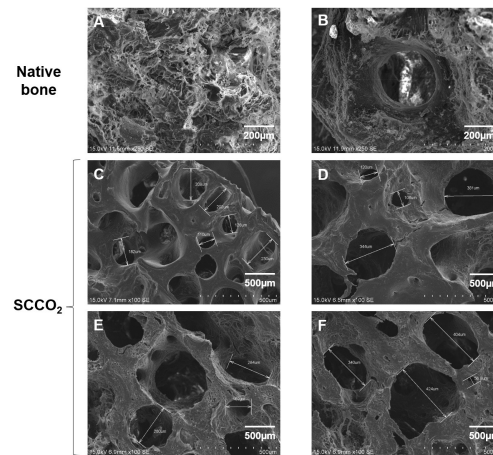

Figure 6. Characterization of SCCO$_2$-processed bone blocks by DNA quantification (**A**) and agarose gel electrophoresis (**B**). Results were expressed as mean ± SD, * $p < 0.001$ were considered statistically significant for different tests (N = 3).

3.2.5. Characterization of SCCO$_2$-Processed Bone Blocks by SEM

To study the surface morphology of SCCO$_2$-processed bone blocks, we analysed the SEM images. The native porcine bone shows cells and cellular debris on the surface of the bone (Figure 7A,B). The SCCO$_2$-processed bone blocks showed no residual cells and soft tissue, and retained the natural pore structure ranging from 100~400 µm (Figure 7C–F) in the bone tissue which is essential for angiogenesis and enhances bone growth. Furthermore, SCCO$_2$-processed bone blocks contained micropores of diameter < 10 µm, which are essential for the transport of body fluids, ion transportation and the attachment of osteoblast suitable for bone regeneration.

Figure 7. Characterization of SCCO2-processed bone blocks by scanning electron microscopy of the native bone block (**A**,**B**) and SCCO2-processed bone blocks (**C–F**).

3.2.6. Mechanical Strength of SCCO2-Processed Bone Blocks

To study the strength and stiffness of SCCO2-processed bone blocks, we analysed the compression test. The test results of SCCO2-processed bone blocks of different sizes showed that they were all greater than the acceptable standard of 2 MPa (Table 1).

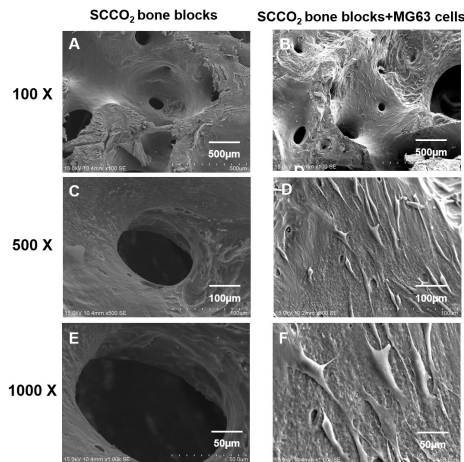**Table 1.** Characterization of SCCO2-processed bone blocks by mechanical stiffness.

SCCO$_2$ Derived Bone Blocks	Mechanical Stiffness (MPa) Mean ± SD
$2 \times 3 \times 2$ cm^3	13.75 ± 3.99
$2 \times 2 \times 2$ cm^3	11.34 ± 1.74
$2 \times 1 \times 2$ cm^3	3.46 ± 3.04
$1 \times 1 \times 2$ cm^3	12.18 ± 1.40

3.2.7. Cell Adhesion and Growth on SCCO2-Processed Bone Blocks by SEM

SEM was performed to evaluate the cell adhesion surface, cell viability and growth of MG63 cells on SCCO2-processed bone blocks. The results show good cell adhesion of MG63 cells on SCCO2-processed bone blocks. In addition, MG63 cells grow well on the surface of the SCCO2-processed bone blocks, the cells were also found to grow inside the pores of SCCO2-processed bone blocks. Overall, the SCCO2-processed bone blocks showed good cell affinity, adhesion and growth even inside the pores after seeding of MG63 cells, which proves excellent cytocompatibility (Figures 8 and 9).
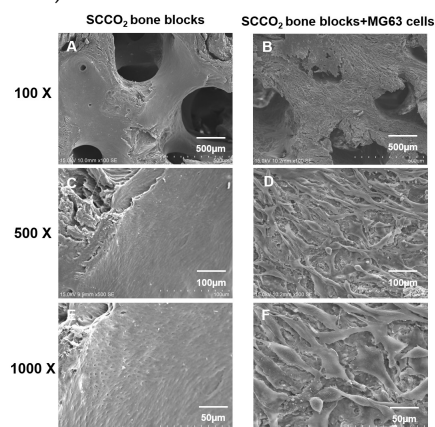
Figure 8. Characterization of SCCO2-processed bone blocks by in vitro cell adhesion and growth on the surface via scanning electron microscopy of the native bone block (**A**,**C**,**E**) and SCCO2-processed bone blocks (**B**,**D**,**F**).

Figure 9. Characterization of SCCO₂-processed bone blocks by in vitro cell growth inside the pores via scanning electron microscopy of the native bone block (**A**,**C**,**E**) and SCCO₂-processed bone blocks (**B**,**D**,**F**).

4. Discussion

Porcine bone xenografts are demonstrated to be an outstanding grafting material for bone augmentation surgeries. The porcine cortical bone used in clinical studies revealed exceptional results and promising clinical application [25]. Already we established the regenerative capability of porcine grafting material such as the cornea, skin matrix and bone can be enhanced by decellularization by employing SCCO₂ extraction technology [26–28] The novel SCCO₂ extraction technique was used to proficiently eliminate the cellular elements of porcine grafting material such as cornea, skin matrix and bone and the biomechanical and biomechanical properties of the graft are well conserved. Furthermore, the decellularized graft material exhibited no immunological reactions, with good biocompatibility and long-term stability [6,7,29,30]. Therefore, in the present study, we used SCCO₂ extraction technology to decellularize the porcine bone after 3D CAD/CAM carving and created a Lego set of the lower jaw, which possesses good biocompatibility and can be used in oral cancer patients where part or full jaw can be replaced.

The bone deformities of the craniofacial skeleton are complex deformities due to congenital abnormalities or from trauma, infection and tumour resection [31]. The reconstruction of these craniofacial bone abnormalities is problematic as these abnormalities are three-dimensional (3D) and complex in size and shape. Until recently, the bone defects have been reconstructed with bone grafts and alloplastic implants. The gold standard for facial reconstruction is the use of autogenous bone [32]. The carving of the bone grafts is performed freehand, which is linked to issues of poor fit within the bone-implant interface, irregular contours, palpable edges and persistent asymmetry [33]. Therefore, in the present study, to obtain a precise bone graft fit with bone interface contact the 3D of the CT image was performed, subsequently mirroring the facial skeleton and finally, modelling and swift prototyping of the left mandibular jaw region were performed.

In the present study, SCCO₂-processed bone blocks were completely decellularized, with the removal of fat and DNA. However, the native collagen scaffold of the SCCO₂-processed bone blocks remains intact and unaltered. Several bone grafts that are accessible in the market are manufactured by a high-temperature sintering process (300–1300 °C), which destroys the collagen scaffold of the bone graft. The conventional decellularization methods employing chemical etching and oxidation methods eliminated only 61% of DNA in porcine decellularized patellar tendons samples [34], and 90% in porcine cartilage and bone [35]. However, the SCCO₂ decellularization method successfully washed off 99.1% DNA in the bone blocks, which has an excellent advantage over the traditional decellularization methods.

In the present study, the SEM revealed that the SCCO₂ process is mild and does not change the native porous structure of bone. The porous nature of the bone plays a vital role in cell seeding diffusion and the mechanical strength of bone graft [36]. The extreme porous nature of the bone graft helps vascularization, osseointegration from native adjacent bone, osteoblast and osteoclast

infiltration to facilitate bone remodelling [37]. The porous nature of the bone graft aids the development of vascular networks to induce the proliferation and differentiation of osteoblasts and enhance the ingrowth of new bone within the bone graft [38]. The $SCCO_2$ process also preserves the diverse range and network of pores from micro- to nanosize which are indispensable in angiogenesis and encourage both bone growth and reorganization in and around the bone graft [39]. The $SCCO_2$ porcine bone graft X-ray diffraction studies revealed an excellent Ca/P ratio of 1.75 as measured employing the wavelength dispersive X-ray fluorescence study, demonstrating the $SCCO_2$ technology preserved the original chemical composition of bone graft which correlates with high levels of Ca and P induces osteogenesis [40].

In the present investigation, $SCCO_2$-processed bone blocks revealed excellent cell adhesion and cytocompatibility with the MG63 cell line examined through SEM. Medical device contamination is routinely assessed which includes the biocompatibility study to appraise the pyrogenic potential of a fever-inducing nature of the product [41]. Our previous $SCCO_2$-processed bone graft studies revealed no signs of adverse effects in cytotoxicity studies in mouse fibroblast L929 cells [6]. The $SCCO_2$-processed bone graft is evidenced to be pyrogen-free. In addition, the $SCCO_2$-derived bone graft is mutagen free, which is evidenced by in vitro gene mutation analysis in L5178Ytk+/− cells. In vivo, systemic toxicity analyses are routinely performed to evaluate a medical device's toxicity related to organs including the liver, heart, kidneys and brain [42]. In conclusion, the $SCCO_2$-processed bone graft proved to be non-toxic and do not have any sign of adverse effects, no mortality and no obvious gross lesions were detected [6,7].

In the current study, $SCCO_2$-processed bone blocks depicted good cytocompatibility along with excellent stiffness in the biomechanical analysis. The conventional decellularization process by chemical detergent and biological agents altered the ECM, the $SCCO_2$-processed bone graft preserved ECM and its mechanical properties [43]. Our previous $SCCO_2$-processed bone graft studies revealed good biocompatibility, healing and bone regeneration in the osteochondral defect model in rabbits. The $SCCO_2$-processed bone graft filled in the defects performed in the distal femoral metaphysis of rabbits, which acts as a bone substitute with absorbable calcium salt and proved to regenerate the bone void with new bone formation indicating $SCCO_2$-processed bone graft possesses excellent osteoconductivity and regenerative potential [6]. The dog's mandibular extraction socket of $SCCO_2$-processed bone graft depicted good bone regeneration was evaluated in our lab. Newly formed bone showed greater stiffness relative to the Bio-Oss®-treated sites in the biomechanical analysis. The $SCCO_2$-processed bone graft depicted more new bone formation and improved bone bridging, than the Bio-Oss® treatment [7].

The clinical studies involving ABCcolla® Collagen Bone Graft which is a $SCCO_2$-processed bone graft from our research group is a strong implant covering the orbital defect with low complication rate, low infection rate, low cost, high biocompatibility and high osteoconductive function [30]. However, preclinical studies depicted that $SCCO_2$-processed bone graft exhibits excellent bone remodelling, regeneration and reabsorption [6,7]. The first clinical study involving orbital wall reconstruction with ABCcolla® Collagen Bone Graft implantation revealed the potential application of the xenograft de-cellular framework to regain functions of orbital walls [30].

In the present study, we used CAD/CAM workflow to reproduce the lower jaw from 3D carving $SCCO_2$-processed Lego bone blocks. End-stage cancer involving the jaws often needs segmental resection. Subsequent reconstruction by free microvascular bone transfer is based on the choice in patients with acceptable health status [44,45]. The CAD-based planning and preoperative manufacturing by CAM of surgical templates to support the surgery of tumours. The CAD-CAM workflow permits the preoperative description of cutting paths and angles at the resection site, modelling of the bone graft as well as the shape of the bone graft leading to an efficient composable and placeable reconstruction. The complete assembly time including the intraoperative cutting, positioning and refinement of the bone graft is decreased by the CAD/CAM workflow [46,47], thereby significantly decreasing the issue associated with long surgery time. In addition, CAD-CAM workflow improves the aesthetic and functional outcome by augmenting the position and contour of the reconstruction [44,46]. In the present study, we CAD-CAM carved the porcine bones into pieces of Lego to form the whole jaw and processed by

SCCO₂ decellularization. To our knowledge, this is the first attempt to create a complete jaw, and it is ready to move into the initial stage of clinical application.

5. Conclusions

This section is not mandatory but can be added to the manuscript if the discussion is unusually long or complex.

References

1. Betz, R.R. Limitations of autograft and allograft: New synthetic solutions. *Orthopaedics* **2002**, *25* (Suppl. 5), 561–570.
2. Kumar, P.; Vinitha, B.; Fathima, G. Bone grafts in dentistry. *J. Pharm. Bioallied Sci.* **2013**, *5* (Suppl. 1), S125–S127.
3. Conrad, E.U.; Gretch, D.R.; Obermeyer, K.R.; Moogk, M.S.; Sayers, M.; Wilson, J.J.; Strong, D.M. Transimission of the hepatitis-C virus by tissue transplantation. *J. Bone Jt Surg. Am.* **1995**, *77*, 214–224.
4. Phelps, A.M. Transplantation of tissue from lower animals to man, and a report of the case of bone-transplantation at Charity Hospital, Black well's Island, N.Y. 1891. *Clin. Orthop. Relat. Res.* **2000**, *371*, 3–9.
5. Fages, J.; Marty, A.; Delga, C.; Condoret, J.S.; Combes, D.; Frayssinet, P. Use of supercritical CO₂ for bone delipidation. *Biomaterials* **1994**, *15*, 650–656.
6. Chen, Y.W.; Hsieh, D.J.; Periasamy, S.; Yen, K.C.; Wang, H.C.; Chien, H.H. Development of a decellularized porcine bone graft by supercritical carbon dioxide extraction technology for bone regeneration. *J. Tissue Eng. Regen. Med.* **2021**, *15*, 401–414.
7. Chen, Y.W.; Chen, M.Y.; Hsieh, D.J.; Periasamy, S.; Yen, K.C.; Chuang, C.T.; Wang, H.C.; Tseng, F.W.; Kuo, J.C.; Chien, H.H. Evaluating the bone-regenerative role of the decellularized porcine bone xenograft in a canine extraction socket model. *Clin. Exp. Dent. Res.* **2021**, *7*, 409–418.
8. Oryan, A.; Alidadi, S.; Moshiri, A.; Maffulli, N. Bone regenerative medicine: Classic options, novel strategies, and future directions. *J. Orthop. Surg. Res.* **2014**, *9*, 18.
9. Fernández, M.P.R.; Gehrke, S.A.; Martinez, C.P.A.; Guirado, J.L.C.; de Aza, P.N. SEM-EDX study of the degradation process of two xenograft materials used in sinus lift procedures. *Materials* **2017**, *10*, 542.
10. Ginebra, M.; Espanol, M.; Maazouz, Y.; Bergez, V.; Pastorino, D. Bioceramics and bone healing. *EFORT Open Rev.* **2018**, *3*, 173–183.
11. Markopoulos, A.K. Current aspects on oral squamous cell carcinoma. *Open Dent. J.* **2012**, *6*, 126–130.
12. Rogers, S.N.; Devine, J.; Lowe, D.; Shokar, P.; Brown, J.S.; Vaugman, E.D. Longitudinal health-related quality of life after mandibular resection for oral cancer: A comparison between rim and segment. *Head Neck* **2004**, *26*, 54–62.
13. Davey, M.; McInerney, N.M.; Barry, T.; Hussey, A.; Potter, S. Virtual Surgical Planning Computer-aided Design-guided Osteocutaneous Fibular Free Flap for Craniofacial Reconstruction: A Novel Surgical Approach. *Cureus* **2019**, *11*, e6256.
14. Antony, A.K.; Chen, W.F.; Kolokythas, A.; Weimer, K.A.; Cohen, M. Use of virtual surgery and stereolithography-guided osteotomy for mandibular reconstruction with the free fibula. *Plast. Reconstr. Surg.* **2011**, *128*, 1080–1084.
15. Jindal, S.K.; Sherriff, M.; Waters, M.G.; Smay, J.E. Development of a 3D printable maxillofacial silicone: Part II. Optimization of moderator and thixotropic agent. *J. Prosthet. Dent.* **2018**, *119*, 299–304.
16. Elbashti, M.; Hattori, M.; Sumita, Y.; Aswehlee, A.; Yoshi, S.; Taniguchi, H. Creating a digitized database of maxillofacial prostheses (obturators): A pilot study. *J. Adv. Prosthodont.* **2016**, *8*, 219–223.

17. Cristache, C.M.; Tudor, I.; Moraru, L.; Cristache, G.; Lanza, A.; Burlibasa, M. Digital Workflow in Maxillofacial Prosthodontics—An Update on Defect Data Acquisition, Editing and Design Using Open-Source and Commercial Available Software. *Appl. Sci.* **2021**, *11*, 973.

18. Sharaf, B.; Levine, J.P.; Hirsch, D.L.; Bastidas, J.A.; Schiff, B.A.; Garfein, E.S. Importance of computer-aided design and manufacturing technology in the multidisciplinary approach to head and neck reconstruction. *J. Craniofac. Surg.* **2010**, *21*, 1277–1280.

19. Bhumiratana, S.; Bernhard, J.C.; Alfi, D.M.; Yeager, K.; Eton, R.E.; Bova, J.; Shah, F.; Gimble, J.M.; Lopez, M.J.; Eisig, S.B.; et al. Tissue-engineered autologous grafts for facial bone reconstruction. *Sci. Transl. Med.* **2016**, *8*, 34–36.

20. Mangano, F.; Zecca, P.; Pozzi-Taubert, S.; Macchi, A.; Ricci, M.; Luongo, G.; Mangano, C. Maxillary sinus augmentation using computer-aided design/computer-aided manufacturing (CAD/CAM) technology. *Int. J. Med. Robot.* **2013**, *9*, 331–338.

21. Liu, Y.F.; Xu, L.W.; Zhu, H.Y.; Liu, S.S. Technical procedures for template-guided surgery for mandibular reconstruction based on digital design and manufacturing. *Biomed. Eng. Online* **2014**, *13*, 63.

22. Figliuzzi, M.; Mangano, F.G.; Fortunato, L.; De Fazio, R.; Macchi, A.; Iezzi, G.; Piattelli, A.; Mangano, C. Vertical ridge augmentation of the atrophic posterior mandible with custommade, computer-aided design/computer-aided manufacturing porous hydroxyapatite scaffolds. *J. Craniofac. Surg.* **2013**, *24*, 856–859.

23. Helal, M.H.; Hendawy, H.D.; Gaber, R.A.; Helal, N.R.; Aboushelib, M.N. Osteogenesis ability of CAD-CAM biodegradable polylactic acid scaffolds for reconstruction of jaw defects. *J. Prosthet. Dent.* **2019**, *121*, 118–123.

24. Wong, T.-Y.; Liu, J.-K.; Fang, J.-J.; Wu, T.-C.; Tu, Y-S. Use of the Matching-Optimal-Symmetry-Plane Method in Planning Surgical Correction of Facial Asymmetry—A preliminary report on 20 patients. *J. Oral Maxillofac. Surg.* **2014**, *72*, 1180.e1–1180.e13.

25. Scarano, A.; Piattelli, A.; Perrotti, V.; Manzon, L.; Iezzi, G. Maxillary Sinus Augmentation in Humans Using Cortical Porcine Bone: A Histological and Histomorphometrical Evaluation after 4 and 6 Months. *Clin. Implant. Dent. Relat. Res.* **2011**, *13*, 13–18.

26. Huang, Y.H.; Tseng, F.W.; Chang, W.H.; Peng, I.C.; Hsieh, D.J.; Wu, S.W.; Yeh, M.L. Preparation of acellular scaffold for corneal tissue engineering by supercritical carbon dioxide extraction technology. *Acta Biomater.* **2017**, *58*, 238–243.

27. Liang, C.M.; Hsieh, D.J.; Tseng, F.W.; Srinivasan, P.; Yeh, M.L.; Tai, M.C. Acellular Porcine Cornea Produced by Supercritical Carbon Dioxide Extraction: A Potential Substitute for Human Corneal Regeneration. *Cornea* **2022**, *41*, 328–338.

28. Chou, P.R.; Lin, Y.N.; Wu, S.H.; Lin, S.D.; Srinivasan, P.; Hsieh, D.J.; Huang, S.H. Supercritical Carbon Dioxide-decellularized Porcine Acellular Dermal Matrix combined with Autologous Adipose-derived Stem Cells: Its Role in Accelerated Diabetic Wound Healing. *Int. J. Med. Sci.* **2020**, *17*, 354–367.

29. Liu, K.F.; Chen, R.F.; Li, Y.T.; Lin, Y.N.; Hsieh, D.J.; Periasamy, S.; Lin, S.D.; Kuo, Y.R. Supercritical Carbon Dioxide Decellularized Bone Matrix Seeded with Adipose-Derived Mesenchymal Stem Cells Accelerated Bone Regeneration. *Biomedicines* **2021**, *9*, 1825.

30. Huang, C.H.; Hsieh, D.J.; Wu, Y.C.; Yen, K.C.; Srinivasan, P.; Lee, H.C.; Chen, Y.C.; Lee, S.S. Reconstruction of the orbital floor using supercritical CO_2 decellularized porcine bone graft. *Int. J. Med. Sci.* **2021**, *18*, 3684–3691.

31. Toth, B.A.; Ellis, D.S.; Stewart, W.B. Computer-designed prostheses for orbitocranial reconstruction. *Plast. Reconstr. Surg.* **1988**, *81*, 315–324.

32. Panicker, P.P.; Mohan, S.P.; Nallusamy, J.; Lakshmi, S.J.; Johny, J.; Bhaskaran, M.K. Reconstruction of Craniofacial Bone Defects with Autologous Human Bone Marrow Stem Cells and Autogenous Bone Grafts: A Case Report with Review of Literature. *J. Pharm. Bioallied. Sci.* **2020**, *12* (Suppl. 1), S394–S398.

33. Lee, S.J.; Lee, H.P.; Tse, K.M.; Cheong, E.C.; Lim, S.P. Computer-aided design and rapid prototyping-assisted contouring of costal cartilage graft for facial reconstructive surgery. *Craniomaxillofac. Trauma Reconstr.* **2012**, *5*, 75–82.

34. Seyler, T.M.; Bracey, D.N.; Plate, J.F.; Lively, M.O.; Mannava, S.; Smith, T.L.; Whitlock, P.W. The development of a xenograft-derived scaffold for tendon and ligament reconstruction using a decellurisation and oxidation protocol. *Arthroscopy* **2017**, *33*, 374–386.

35. Elder, S.; Chenault, H.; Gloth, P.; Webb, K.; Recinos, R.; Wright, E.; Cooley, A. Effects of antigen removal on a porcine osteochondral xenograft for articular cartilage repair. *J. Biomed. Mater. Res. A* **2018**, *106*, 2251–2260.

36. Bertoldi, S.; Fare, S.; Tanzi, M.C. Assessment of scaffold porosity: The new route of micro-CT. *J. Appl. Biomech.* **2011**, *9*, 165–175.

37. Bracey, D.N.; Seyler, T.M.; Jinnah, A.H.; Lively, M.O.; Willey, J.S.; Smith, T.L.; Whitlock, P.W. A decellularized porcine xenograftderived bone scaffold for clinical use as a bone graft substitute: A critical evaluation of processing and structure. *J. Funct. Biomater.* **2018**, *9*, 45.

38. Vilela, M.J.C.; Colaço, B.J.A.; Ventura, J.; Monteiro, F.J.M.; Salgado, C.L. Translational Research for Orthopedic Bone Graft Development. *Materials* **2021**, *14*, 4130.

39. Ling, Y.; Xu, W.; Yang, L.; Liang, C.; Xu, B. Improved the biocompatibility of cancellous bone with compound physicochemical decellurisation process. *Regen. Biomater.* **2020**, *7*, 443–451.

40. Maté Sánchez de Val, J.E.; Calvo-Guirado, J.L.; Gómez-Moreno, G.; Pérez- Albacete Martínez, C.; Mazón, P.; De Aza, P.N. Influence of hydroxyapatite granule size, porosity, and crystallinity on tissue reaction in vivo. Part A: Synthesis, characterization of the materials, and SEM analysis. *Clin. Implant Dent. Relat. Res.* **2016**, *27*, 1331–1338.

41. de Almeida, C.S.; Sartoretto, S.C.; Durte, I.M.; Alves, A.T.N.N.; Barreto, H.V.; Resende, R.F.B.; Calasans-Maia, M.D.; de Albuquerque, J.C. In Vivo Evaluation of Bovine Xenograft Associated with Oxygen Therapy in Alveolar Bone Repair. *J. Oral Implantol.* **2021**, *47*, 465–471.

42. International Organisation for Standardisation [ISO]. ISO 10993-11: Biological Evaluation Of Medical Devices—Part 11 Tests for Systemic Toxicity. 2017. Available online: http://nhiso.com/wp-content/uploads/2018/05/ISO-10993-11-2017.pdf (accessed on 10 February, 2022).

43. Gilpin, A.; Yang, Y. Decellurisation strategies for regenerative medicine: From processing techniques to applications. *Biomed. Res. Int.* **2017**, *2017*, 9831534.

44. Goetze, E.; Gielisch, M.; Moergel, M.; Al-Nawas, B. Accelerated workflow for primary jaw reconstruction with microvascular fibula graft. *3D Print Med.* **2017**, *3*, 3.

45. Gerressen, M.; Pastaschek, C.I.; Riediger, D.; Hilgers, R.D.; Hölzle, F.; Noroozi, N.; Ghassemi, A. Microsurgical Free Flap Reconstructions of Head and Neck Region in 406 Cases: A 13-Year Experience. *J. Oral Maxillofac. Surg.* **2013**, *71*, 628–635.

46. Rodby, K.A.; Turin, S.; Jacobs, R.J.; Cruz, J.F.; Hassid, V.J.; Kolokythas, A.; Antony, A.K. Advances in oncologic head and neck reconstruction: Systematic review and future considerations of virtual surgical planning and computer aided design/computer aided modeling. *J. Plast. Reconstr. Aesthet. Surg.* **2014**, *67*, 1171–1185.

47. Sieira Gil, R.; Roig, A.M.; Obispo, C.A.; Morla, A.; Pages, C.M.; Perez, J.L. Surgical planning and microvascular reconstruction of the mandible with a fibular flap using computer-aided design, rapid prototype modelling, and precontoured titanium reconstruction plates: A prospective study. *Br. J. Oral Maxillofac. Surg.* **2015**, *53*, 49–53.

綠茵生技股份有限公司

企業簡介

綠茵生技成立於 2012 年，為國際生技食品原料研發生產大廠。綠茵生技為綠茵集團母公司，旗下有國外獨家品牌保健食品原料代理**康普森生技**與 ODM 產品研發設計代工之鋒揚生醫。

綠茵生技研發具台灣特色與國際競爭力之保健原料，並提供專業一站式客製化代工服務，替客戶打造高功效與市場差異化保健品。

綠茵目前每年服務數百位國內、外客戶，已成功打造上千款熱銷產品，並透過專業營養師與行銷團隊替客戶加值品牌產品競爭力。

綠茵獲得多項國際食品品質系統認證包含 FSSC 22000、ISO 22000、HACCP、TQF、GMP、HALAL 與 ISO/IEC 17025 認證實驗室等認證。

保健原料代理
康普森生技
代理百種以上國際知名
保健品牌原料

保健食品代工廠
鋒揚生醫
提供劑型設計、高品質管控代
工、教育訓練等服務

生技原料研發製造廠
綠茵生技
研發潛力台灣特色保健原料
佈局國際

經營理念

主要有二：

◆ 突破現今生技原料市場中，具市場高度需求、但至今生物科技仍未能達到的技術與產品

◆ 整合台灣在國際上領先的技術與產品，使其得以獲國際主流市場的廣泛接受

綠茵生技以**「創新研發」**、**「精準優化」**、**「整合行銷」**作為三大經營發展主軸，整合全球**「產」**、**「經」**、**「學」**、三方資源，運用豐富的市場營銷經驗、長期的產學合作機制、堅實的技術研發團隊，洞悉市場需求與投入研究計畫，將研發成果快速產業化。

精準計算與持續優化「規格、成本、數據」，達到出口國際主流市場的五大條件：**「國際認證」**、**「臨床試驗」**、**「全球專利」**、**「超越規格」**、**「合宜價格」**，提供客戶高 CP 值的產品與服務。

生產基地

綠茵生技目前有兩座生產基地，綠茵一廠於 2013 年通過政府審核，獲准設立于知名的創新產業孵化基地-臺灣中部科學園區，廠房內部設有大型的現代化真菌培養中心生產專利固態培養牛樟芝菌絲體。綠茵二廠於 2017 年落成於台中工業園區，專職生產苦瓜胜肽、蔬果酵素、納豆激酶等生技保健產品。

綠茵生技一廠

綠茵生技二廠

研發中心

集合國內醫學、生物科技、食品領域頂尖學者專家，組成實力堅強的綠茵研發團隊，以獨家專利技術、專屬菌種篩選平臺、現代化真菌培養中心、尖端發酵科技、優異水解工藝、超效能無毒環保萃取制程等，達成高機能成分、高生物利用率、高食用安全的保健原料。

多數原料皆以科學化驗證功效，包含動物試驗、人體實驗以佐證產品功效，並充分整合運用生技研究資源，共創生技原料新價值，並向全球市場邁進。

廠區認證

綠茵生技高規格廠商並已通過**TQF、ISO22000、FSSC22000、HACCP、HALAL**等國際標準認證，提供客戶最安心的保證。

臺灣優良食品驗證制度(TQF)　　　　清真認證 HALAL

食品安全系統驗證　　食品安全衛生管理驗證　　危害分析重要管制點
FSSC22000　　　　　**ISO22000**　　　　　　**HACCP**

獲獎與榮耀

◆　囊括世界三大發明展金牌、銀牌及特別獎大獎

◆　國家發明獎、專利獎與生技大獎

德國紐倫堡　　瑞士日內瓦　　美國匹茲堡

發明展　　　　發明展　　　　發明展

TSCFA 台灣超臨界流體協會
Taiwan Supercritical Fluid Association

(日間班)高壓氣體特定設備操作人員安全衛生教育訓練班

需要有操作證照的單位，歡迎向協會報名。

● 上課日期：**111/08/15~08/19 08:00~17:00；08/18~08/19 08:00~17:00(實習)**

● 上課時數：高壓氣體特定設備操作人員安全衛生教育訓練課程時數 35 小時＋
2 小時(測驗)。

● 課程內容：高壓氣體概論 3HR、種類及構造 3HR、附屬裝置及附屬品 3HR、
自動檢查與檢點維護 3HR、安全裝置及其使用 3HR、操作要領與
異常處理 3HR、事故預防與處置 3HR、安全運轉實習 12HR、高壓
氣體特定設備相關法規 2HR，共 35 小時。(另加學科測驗 1 小時
及術科測驗約 1~2 小時)

● 上課地點：高雄市楠梓區高楠公路 1001 號【金屬工業研究發展中心研發大樓
2 樓　產業人力發展組】

● 參加對象：從事高壓氣體特定設備操作人員或主管人員。

● 費　　用：本班研習費新台幣 **7,000 元整，本會會員享九折優惠。**

● 名　　額：每班 30 名，額滿為止。

● 結訓資格：期滿經測驗成績合格者，取得【高壓氣體特定設備操作人員安全
衛生訓練】之證書。

● 報名辦法：1.傳真報名：(07)355-7586 台灣超臨界流體協會
2.報名信箱：tscfa@mail.mirdc.org.tw
3.研習費請電匯至 兆豐國際商銀 港都分行(代碼017)
戶名：社團法人台灣超臨界流體協會 帳號：002-09-018479（註明
參加班別及服務單位）或以劃線支票抬頭寫「台灣超臨界流體協會
」連同報名表掛號郵寄台灣超臨界流體協會，本會於收款後立即開
收據寄回。

※洽詢電話：(07)355-5706 吳小姐 繳交一吋相片一張及身份證正本

報　名　表

課程名稱	高壓氣體特定設備操作人員安全衛生教育訓練			上課日期	111 年 08/15~08/19	
姓　　　名	出生年月日	身份證字號	手機號碼	畢業校名		公司產品

服務單位		電　　話	
服務地址	□□□	傳　　真	
發票住址	□□□	統一編號	

負責人	人	訓練聯絡人 / 職稱	email：	
參加費用	共　　　　　　　　　元	參加性質	□公司指派　　　　□自行參加	
繳費方式	□郵政劃撥　　□支票　　□附送現金	報名日期	年　　月　　日	

※ 出生年月日、身份證字號、畢業校名、電話、地址須詳填，以利製作證書。〔！〕

上課日期時間表

課程名稱：(日間班)高壓氣體特定設備操作人員安全衛生教育訓練班

2022/08/15 (一)	08:00～17:00
2022/08/16 (二)	08:00～17:00
2022/08/17 (三)	08:00～17:00
2022/08/18 (四)	08:00～17:00 (實習第 1 組)
2022/08/19 (五)	08:00～14:00 (實習第 1 組)

亞果生醫亮眼新產品 iMist 愛眼濕 亞洲生技展搶眼亮相

2022/07/27

經濟日報 吳國棟

現代人常使用 3C 產品，學生在家線上學習，不自覺用眼過度，常感覺眼睛酸澀、疲勞，市面上也因而有許多護眼產品。亞果生醫利用專利技術 超臨界 二氧化碳去細胞技術，保留完整三股螺旋的膠原蛋白，以高修護性的 AD 膠原蛋白作為原料，生產出新一代 iMist 愛眼濕膠原蛋白保濕噴霧，當眼睛感到不適時，隨時噴一下，就能得到舒緩。

亞果生醫請到台灣小姐邱怡澍為新產品的代言人，邱怡澍說：「五月跟著白沙屯媽祖繞境時，現場信眾熱情，香灰也很多，戴隱形眼鏡的我常感到眼睛不適，這時候 iMist 就發揮很大的功效，小小一瓶隨時噴一下急救，不會耽誤繞境進行影響拍攝，又能馬上舒緩眼睛的不適感，天氣炎熱也感覺眼周肌膚有適時地補水。」

亞果生醫執行長謝達仁表示：「iMist 愛眼濕主要成分是高濃度的活性膠原蛋白，所以一噴就能舒緩眼睛疲勞與乾澀，讓雙眼明亮動人。」

在 7 月 28 日-31 日亞洲生技大展的現場，提供 iMist 愛眼濕新品上市買一送一的優惠，攤位上(號碼 R519)還有同樣使用亞果生醫高品質膠原蛋白的 ACRODERM 保養品，讓民眾可以到現場體驗試用，將最新的產品以優惠價帶回家，詳情請洽官方 LINE@ACRODERM。

資料來源：https://money.udn.com/money/story/12331/6492742?from=edn_search_result

A Comparative Assessment on Different Aspects of the Non-Linear Instability Dynamics of Supercritical Fluid in Parallel Channel Systems

平行通道系統中超臨界流體非線性不穩定性動力學不同方面的比較評估

by **Munendra Pal Singh** [1,*], **Abdallah Sofiane Berrouk** [1,2] and **Suneet Singh** [3]

[1] Department of Mechanical Engineering, Khalifa University of Science and Technology, Abu Dhabi 127788, United Arab Emirates

[2] Center for Catalysis and Separations (CeCas), Khalifa University of Science and Technology, Abu Dhabi 127788, United Arab Emirates

[3] Department of Energy Science & Engineering, Indian Institute of Technology Bombay, Mumbai 400076, India

Abstract

The thermal-hydraulic behavior of supercritical water reactors with a parallel channel configuration was examined through a non-linear instability analysis. This analysis was performed under wide-ranging conditions and aspects, including different working supercritical fluids, varied heat-flux and flow-rate conditions, and channel inclinations. The supercritical fluid (SCFs) dynamics were captured using the density, enthalpy, and velocity analytical approximation functions. The major findings show that both SCFs (water and carbon dioxide) experienced density wave oscillations at a low pseudo-subcooling number. Static instability characteristics were observed for supercritical water, at a relatively high subcooling number. Further, it was found that at different heat flux, the hotter channel makes the overall system more unstable, whereas, at equal heat flux, parallel channels perform similar to a single-channel system. However, the effect of the inclination angle was found to be negligible owing to supercritical pressure conditions. Moreover, stable and unstable limit cycles along with out-of-phase oscillation characteristics were observed in dynamic stability regions. The present model was also compared with experimental and numerical data. Moreover, co-dimension and numerical simulations were performed to confirm the observed non-linear characteristics. This study helps to enhance the heat transfer characteristics during safe operation of heated channel systems, such as nuclear reactors and solar thermal systems. **View Full-Text**

Keywords: supercritical fluid; non-linear stability analysis; nuclear reactor; Ledinegg instability; Hopf bifurcation

Discovery of Stishovite in the Prismatine-Bearing Granulite from Waldheim, Germany: A Possible Role of Supercritical Fluids of Ultrahigh-Pressure Origin

在德國瓦爾德海姆含棱晶石的花崗岩中發現 Stishovite：超高壓源超臨界流體的可能作用

by **Rainer Thomas** [1,*], **Paul Davidson** [2], **Adolf Rericha** [3] and **Ulrich Recknagel** [4]

[1] Im Waldwinkel 8, D-14662 Friesack, Germany

[2] Codes, Centre for Ore Deposits and Earth Sciences, University of Tasmania, Hobart, Australia

[3] Alemannenstraße 4a, D-144612 Falkensee, Germany

[4] Böhmerwaldstraße 22, D-86529 Schrobenhausen, Germany

Abstract

For the first time in the sixty years since the synthesis of stishovite, we report unambiguous evidence of stishovite formed in the deep Earth. A minimum pressure of about 7.5 GPa at 1000 °C is necessary for the formation of stishovite, corresponding to a depth of about 230 km. In this manuscript we report the identification of stishovite along with coesite as inclusions in mineral grains from the Waldheim granulite. This implies that the stishovite was transported upwards, probably very rapidly to a depth of about 130 km, corresponding to the highest pressure indicated by newly identified coesite in the prismatine of the Waldheim granulite, and continuing up to the depth of emplacement of the Waldheim prismatine granulite. The analysis of the Raman spectra obtained from a metastable trapped stishovite micro-crystal show that all the diagnostic Raman bands are present. However, given the metastability of the stishovite at room temperatures and pressures, this mineral breaks down step-by-step into stable polymorphs, first coesite and then quartz and cristobalite, during the Raman stimulation. The rare coesite crystals in prismatine have also resulted from the irreversible transformation from stishovite. Although the Waldheim occurrence may be unique, we suggest that Raman analysis of co-trapped crystals in similar deep-seated rocks, an area of limited previous research, may prove an important innovation in the study of mantle processes. **View Full-Text**

Experimental Investigations on Thermal-Hydraulics of Supercritical Carbon Dioxide Under Natural Circulation Vertical Flows

自然循環垂直流下超臨界二氧化碳熱流試驗研究

by Kapil Bodkha, D. S. Pilkhwal, N. K. Maheshwari

Kapil Bodkha

Engineering Sciences Discipline, Homi Bhabha National Institute, Mumbai 400094, India;
Reactor Design & Development Group, Bhabha Atomic Research Centre, Mumbai 400085, India

D. S. Pilkhwal

Cryo-Technology Division, Bhabha Atomic Research Centre, Mumbai 400085, India

N. K. Maheshwari

Reactor Design & Development Group, Bhabha Atomic Research Centre, Mumbai 400085, India

Abstract

Advanced energy systems propose use of supercritical fluids (SCFs) as working fluids owing to various advantages associated with SCF. Supercritical water (SCW), supercritical carbon-dioxide (SC–CO_2), and supercritical helium (SC–He) find proposed applications in advanced nuclear reactor designs too. Heat transfer behavior of SCFs is still not understood completely. Though there exist many heat transfer correlations and criterion in the literature, they miss having a general consensus among them. In spite of having many reported studies in literature for SCFs under forced convection conditions, studies related to SCF under natural circulation (NC) mode are very limited. In the present study, extensive experiments have been performed with SC–CO_2 under NC conditions in tube geometry. The experimental data generated for vertical heated test section at various pressures between 8.0 and 13.0 MPa have been utilized to bring out salient findings related to fluid flow and heat transfer. The data have also been utilized to make comparison with generalized NC flow correlation available in the literature. Besides, few popular heat transfer correlations have been compared with experimentally obtained heat transfer coefficients.

Keywords: supercritical carbon-dioxide, natural circulation, heat transfer, vertical section, fluid flow, experiments

Lipid Extracts Obtained by Supercritical Fluid Extraction and Their Application in Meat Products

超臨界流體萃取獲得的脂質提取物及其在肉製品中的應用

by **Branislav Šojić** [1], **Predrag Putnik** [2], **Bojana Danilović** [3], **Nemanja Teslić** [4], **Danijela Bursać Kovačević** [5,*] and **Branimir Pavlić** [1,*]

[1] Faculty of Technology, University of Novi Sad, 21000 Novi Sad, Serbia

[2] Department of Food Technology, University North, 48000 Koprivnica, Croatia

[3] Faculty of Technology, University of Niš, 16000 Leskovac, Serbia

[4] Institute of Food Technology, University of Novi Sad, 21000 Novi Sad, Serbia

[5] Faculty of Food Technology and Biotechnology, University of Zagreb, Zagreb, Croatia

Abstract

Supercritical fluid extraction (SFE) has been recognized as the green and clean technique without any negative impact on the environment. Although this technique has shown high selectivity towards lipophilic bioactive compounds, very few case studies on the application of these extracts in final products and different food matrices were observed. Considering the recent developments in food science and the increasing application of supercritical extracts in meat products in the last decade (2012–2022), the aim of this manuscript was to provide a systematic review of the lipid extracts and bioactives successfully obtained by supercritical fluid extraction and their application in meat products as antioxidant and/or antimicrobial agents. Lipophilic bioactives from natural resources were explained in the first step, which was followed by the fundamentals of supercritical fluid extraction and application on recovery of these bioactives. Finally, the application of natural extracts and bioactives obtained by this technique as functional additives in meat and meat products were thoroughly discussed in order to review the state-of-the-art techniques and set the challenges for further studies. **View Full-Text**

Numerical investigation of heat transfer deterioration and the variation of Prandtl number in the main flow area under supercritical conditions

超臨界條件下主流區傳熱劣化及普朗特數變化的數值研究

by Zilun Zeng [a], Chao Wang [a], Yuhang Li [a], Hasan Izhar Khan [b], **Hongyuan Li** [a] & Hong Xu [a]

[a] MOE's Key Lab of Power Station Energy Transfer Conversion and System, School of Energy, Power and Mechanical Engineering, North China Electric Power University, Beijing

[b] Department of Mechanical Engineering, University of Engineering and Technology, Lahore, Punjab, Pakistan

Abstract

The problem of heat transfer deterioration (HTD) exists in supercritical conditions of the power plant during peak operation. The turbulence model is selected to be applicable to the cross-critical flow field, and the different simulation models results are compared with the Yamagata experimental data. The different inner diameters and heat fluxes have a significant effect on the HTD, accompanied by variation in the Prandtl number change rate. This change can be expressed by the full width at half maximum of the Pr number along the bulk fluid enthalpy. It is analyzed that the HTD is related to the layer difference between the temperature boundary layer and velocity boundary layer, and to the decrease of the thermal conductivity inside the temperature boundary layer near the wall.

Keywords: Boundary layer, heat transfer deterioration, Prandtl number, turbulence model

資料來源：https://doi.org/10.1080/10407782.2022.2079288

Production of Protein Hydrolysate from Quinoa (*Chenopodium quinoa* Willd.): Economic and Experimental Evaluation of Two Pretreatments Using Supercritical Fluids' Extraction and Conventional Solvent Extraction

從藜麥（ *Chenopodium quinoa* Willd.） 中生產蛋白質水解物：使用超臨界流體萃取和常規溶劑萃取兩種預處理的經濟和實驗評估

by **Luis Olivera-Montenegro** [1,*], **Alejandra Bugarin** [1], **Alejandro Marzano** [1], **Ivan Best** [1], **Giovani L. Zabot** [2] and **Hugo Romero** [3]

[1] Grupo de Ciencia, Tecnología e Innovación en Alimentos, Universidad San Ignacio de Loyola, Lima 15024, Peru

[2] Laboratory of Agroindustrial Processes Engineering (LAPE), Federal University of Santa Maria (UFSM), 1040 Sete de Setembro St., Center DC, Cachoeira do Sul 96508-010, RS, Brazil

[3] Electroanalytical Applications and Bioenergy Research Group, Chemical Engineering Department, Technical University of Machala, Av. Panamericana Km 5 ½, Machala, Ecuador

Abstract

Supercritical fluids' extraction (SFE) and conventional solvent extraction (CSE) for defatting of quinoa flour as pretreatments to produce the quinoa protein hydrolysate (QPH) were studied. The objective was to extract the oil and separate the phenolic compounds (PC) and the defatted quinoa flour for subsequent quinoa protein extraction and enzymatic hydrolysis. The oil extraction yield (OEY), total flavonoid content (TFC), and QPH yield were compared. SuperPro Designer 9.0® software was used to estimate the cost of manufacturing (COM), productivity, and net present value (NPV) on laboratory and industrial scales. SFE allows higher OEY and separation of PC. The SFE oil showed a higher OEY (99.70%), higher antioxidant activity (34.28 mg GAE/100 g), higher QPH yield (197.12%), lower COM (US\$ 90.10/kg), and higher NPV (US\$ 205,006,000) as compared to CSE (with 77.59%, 160.52%, US\$ 109.29/kg, and US\$ 28,159,000, respectively). The sensitivity analysis showed that the sale of by-products improves the economic results: at the industrial scale, no significant differences were found, and both processes are economically feasible. However, results indicate that SFE allows the recovery of an oil and QPH of better nutritional quality and a high level of purity-free organic solvents for further health and nutraceutical uses. **View Full-Text**

Keywords: quinoa oil; bioactive peptides; SFE; economic evaluation; quinoa protein hydrolysate